


Anisotropic signatures of electron hydrodynamics

Jorge Estrada-Álvarez ^{*}, Francisco Domínguez-Adame , and Elena Díaz 
 GISC, Departamento de Física de Materiales, Universidad Complutense, E-28040 Madrid, Spain

 (Received 25 October 2024; accepted 2 January 2025; published 23 January 2025)

Electron hydrodynamics refers to the transport regime where electrons collectively behave like a fluid. Its realization requires pure materials, some of which, such as bilayer graphene or PdCoO₂, are anisotropic so that different in-plane transport directions can be defined. Collective electron flow also benefits from geometrically engineered devices because it is highly dependent on the nonuniformity of the electron flow. Here we analyze carrier transport in anisotropic materials where remarkable effects emerge after the proper directional design of the device. Simulations based on the Boltzmann transport equation demonstrate that electrical properties are clearly different when the device is set in the easy or the hard transport directions, namely, when the transport channel is aligned or not aligned to the group velocity at the Fermi level, respectively. Most importantly, the standard signatures of viscous electron flow, such as Poiseuille flow, superballistic conduction, and the formation of whirlpools, are enhanced when the anisotropic device operates in the hard transport directions. As a result, we demonstrate that electron hydrodynamics leads to a different route for efficient charge transport in the hard in-plane transport directions.

DOI: [10.1103/PhysRevResearch.7.013087](https://doi.org/10.1103/PhysRevResearch.7.013087)

I. INTRODUCTION

The pursued miniaturization of electronics, counting the use of two-dimensional (2D) devices, faces assorted difficulties [1]. As such, energy dissipation, with its environmental ramifications, is paramount. One way to deal with energy losses is to exploit the emerging transport regimes in 2D materials. This is the case of hydrodynamics, where electrons move collectively, such as in a conventional viscous fluid [2–5], giving rise to exotic hydrodynamic signatures. The most remarkable are (i) the Poiseuille flow in channels, such that central electrons move faster, leading to a transversal curve profile [6], (ii) the superballistic conduction or Gurzhi effect [7–13], and (iii) the emergence of whirlpools and negative resistances in symmetry-broken devices, associated with the finite viscosity of the electron fluid [14–17]. Superballistic conduction is very promising in the field of electronics. Here the effect of a finite temperature enhances electron-electron collisions, favoring a collective behavior where electrons dodge the edges of the sample. Accordingly, the resistance falls under the ballistic limit, a convenient property to reduce energy dissipation. Further interest in electron hydrodynamics stems from its applications in amplifying or oscillating circuits [18,19], aside from the cornerstone of low-energy dissipation [13,20].

The first strategies for the realization of electron hydrodynamics were based on pure 2D materials, including graphene [6,15,17] and 2D GaAs [8]: electrons travel long distances until they scatter against impurities or phonons, showing their underlying collective properties. This is also the case of bilayer graphene [15], an anisotropic material where, for a certain filling of the band structure, most of the electrons will only propagate in six directions. Moreover, three of them correspond to one valley and three to the other, so that the anisotropic properties may be used for valleytronics [21–23]. Further systems to be studied are semimetals and the delafossites PtCoO₂ and PdCoO₂ [24], which are layered crystal with sheets of platinum and palladium, respectively [25,26]. The features of the out-of-plane band structure of PdCoO₂ ensure a mainly 2D transport and allows us to work with the in-plane approximation. In addition, the purity of this material enables electrons to travel for very long distances [27], namely, 20 μm, before they scatter with an impurity. This makes PdCoO₂ a great candidate to build electronic devices with reduced energy dissipation, where a hydrodynamic response may arise [24,28–31]. Its in-plane Fermi surface is also highly anisotropic [1,30,32–36], with electrons moving in six directions. Although Neumann’s principle predicts an isotropic in-plane resistance of a bulk sample with hexagonal symmetry [1,36,37], the geometry of the device fixes the transport direction and breaks that symmetry. Therefore, the resistance of a PdCoO₂ channel is highly anisotropic: transport is easy if the axis of the channel matches one of the six electron’s velocities, but it is hard if it does not, as we depict in Fig. 1. The latter situation leads to an increased electrical resistance.

Alternative strategies for electron hydrodynamics were based on nanostructuring the devices. The viscous properties emerge when the electron flow is nonhomogeneous, and

^{*}Contact author: jorgestr@ucm.es

Published by the American Physical Society under the terms of the [Creative Commons Attribution 4.0 International license](https://creativecommons.org/licenses/by/4.0/). Further distribution of this work must maintain attribution to the author(s) and the published article’s title, journal citation, and DOI.

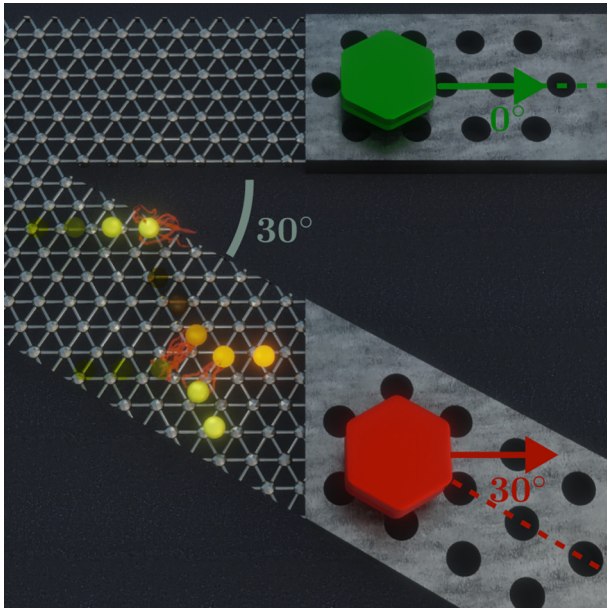


FIG. 1. Anisotropic electron transport. Electrons in PdCoO₂ preferably move in six directions, perpendicular to the Fermi surface and defined by the atomic structure of the palladium planes (not to scale). Collisions against the boundaries increase the resistance, but they can be mitigated with electron-electron collisions. The orientation of the Fermi surface and the geometry, either in a channel or in a honeycomb antidot superlattice, defines easy (0°) and hard (30°) transport directions.

geometrically engineering the device is the best way to bend the electron trajectories. For example, superballistic conduction has been reported in point contacts [7], crenelated channels [8], and antidot superlattices [12], and the more that we bend the flow, the stronger the superballistic effect is. Also, symmetry-broken devices have been considered, leading to the formation of unexpected electronic whirlpools [14,17]. Notice that in sum, the first strategy drove us to anisotropic materials such as PdCoO₂ and the second to geometrically engineered devices with well-defined transport directions. However, to the best of our knowledge, former studies of PdCoO₂ were mostly limited to trivial geometries [38]. In other words, the question of how the material anisotropy can affect viscous electron flow in geometrically engineered devices remains open.

In this paper, we analyze the most relevant signatures to establish viscous electron flow in 2D anisotropic devices: Poiseuille flow, the superballistic conduction, and the formation of whirlpools in symmetry-broken devices. We solve the Boltzmann transport equation in devices working in the easy and the hard flow directions by properly setting the angle between the material Fermi surface and the direction of transport (see Fig. 1). We find that when the device works in the hard flow directions, the three hydrodynamic signatures considered here are enhanced.

II. MODEL

Let us introduce the model to describe a 2D electron system in an anisotropic material [39]. We consider electrons

as semiclassical particles with a steady distribution function $f(\mathbf{r}, \mathbf{k})$ such that $f(\mathbf{r}, \mathbf{k}) d^2\mathbf{r} d^2\mathbf{k}$ is the number of electrons around position \mathbf{r} and momentum $\hbar\mathbf{k}$. The dynamics of the electrons when they are subjected to an electric potential $V(\mathbf{r})$ and a perpendicular magnetic field \mathbf{B} can be described by the following Boltzmann transport equation [1,39–42]:

$$\mathbf{v} \cdot \nabla_{\mathbf{r}} f + \frac{e}{\hbar} (\nabla_{\mathbf{r}} V - \mathbf{v} \times \mathbf{B}) \cdot \nabla_{\mathbf{k}} f = \Gamma[f], \quad (1)$$

where e is the elementary charge and \hbar is the reduced Planck's constant. We consider the following arbitrary Fermi surface [1]:

$$k_F(\theta) = k_F \rho(\theta) \begin{pmatrix} \cos \theta \\ \sin \theta \end{pmatrix}, \quad (2)$$

where θ is the angle of the electron's momenta, k_F is the Fermi wave number, and $\rho(\theta)$ is a function with a mean value of 1. For PdCoO₂, we assume the hexagon $\rho(\theta) = 1 + 0.034 \cos(6\theta)$ [36]. Thus, the group velocity of the carriers near the Fermi surface is

$$\mathbf{v}(\theta) = v_F \begin{pmatrix} \cos(\theta) \rho(\theta) + \sin(\theta) \partial_{\theta} \rho(\theta) \\ \sin(\theta) \rho(\theta) - \cos(\theta) \partial_{\theta} \rho(\theta) \end{pmatrix}, \quad (3)$$

where v_F is the Fermi velocity. The latter is perpendicular to the Fermi surface and has modulus $v \simeq v_F$ provided that $|\rho - 1| \ll 1$. Note that in the considered case, the anisotropic response of the material is not founded on the change of the modulus of the velocity of the charge carriers, but rather on the change of its direction. Indeed, the hexagonal shape of the Fermi surface forces many electrons to move perpendicular to the sides of the hexagon (easy transport directions), while there are few electrons moving in other directions (hard transport directions). The collision operator $\Gamma[f]$ in Eq. (1) reads

$$\Gamma[f] = -\frac{f - f_e}{l_e v_F^{-1}} - \frac{f_{ee}^{\text{even}} - f_{ee}^{\text{even}}}{l_{ee}^{\text{even}} v_F^{-1}} - \frac{f_{ee}^{\text{odd}} - f_{ee}^{\text{odd}}}{l_{ee}^{\text{odd}} v_F^{-1}}. \quad (4)$$

The first term describes electron scattering against impurities and phonons, where momentum is not conserved. Therefore, the distribution decays to the Fermi equilibrium distribution $f_e(\mathbf{k})$, and the decay ratio is defined with the mean free path l_e . For the purposes of this work, we consider that the easy and hard transport directions are mainly determined by the shape of the Fermi surface and, as such, we take a uniform mean free path l_e . Notice that despite the increase in l_e , for a very few electrons near the vertices of the Fermi surface in PdCoO₂ [24], this is a sensible approximation to determine the overall electrical response for all in-plane electrons [36]. The second term in Eq. (4) describes collisions with other electrons, which are processes that conserve momentum. Hence, the distribution decays to a shifted equilibrium distribution $f_{ee}(\mathbf{r}, \mathbf{k}) = f_e[\mathbf{k} - \bar{\mathbf{k}}(\mathbf{r})]$, where $\bar{\mathbf{k}}(\mathbf{r}) = (1/n) \int \mathbf{k} f(\mathbf{r}, \mathbf{k}) d^2\mathbf{k}$ is the mean wave number and $n = \int f(\mathbf{r}, \mathbf{k}) d^2\mathbf{k}$ is the density of carriers, which is uniform in the sample. We shall use a more realistic approach than Callaway's ansatz [43] by taking different l_{ee}^{even} and l_{ee}^{odd} for the modes of the polar expansion of f with even and odd indexes, respectively. In particular, we assume $l_{ee} = l_{ee}^{\text{even}} \ll l_{ee}^{\text{odd}}$, which gives rise to the so-called tomographic regime [44–46].

Transport phenomena happen near the Fermi surface and they can be described using a reduced distribution function $g(\mathbf{r}, \theta) = 4\pi^2 v_F k_F^{-1} \int_0^\infty (f - f_e) dk$, which only depends on the polar angle θ and splits into its even- and odd-parity parts. After definition of $g_{ee}(\mathbf{r}, \theta) = 4\pi^2 v_F k_F^{-1} \int_0^\infty (f_{ee} - f_e) dk$, we assume linear transport with $g \ll v_F$ and $|\rho - 1| \ll 1$, so that Eq. (1) reduces to

$$\begin{aligned} & \frac{\mathbf{v}(\theta)}{v_F} \cdot \nabla_r g - \frac{e}{\hbar k_F} \nabla_r V + \frac{\partial_\theta g}{l_B} \\ &= -\frac{g}{l_e} - \frac{g_{ee}^{\text{even}} - g_{ee}^{\text{even}}}{l_{ee}^{\text{even}}} - \frac{g_{ee}^{\text{odd}} - g_{ee}^{\text{odd}}}{l_{ee}^{\text{odd}}}, \end{aligned} \quad (5)$$

where $l_B = \hbar k_F / eB$ is the cyclotron radius. Finally, the drift velocity is computed as

$$\mathbf{u} = \frac{1}{\pi} \int \mathbf{v}(\theta) g(\theta) d\theta. \quad (6)$$

Equation (5) must be solved for an appropriate edge scattering [39,47]. In particular, we study the two most commonly accepted boundary conditions. First is a fully diffusive boundary (DF), assuming $g(\theta) = 0$ for all the scattered directions. This means the electrons scatter uniformly in all directions, regardless of the incident distribution on a wall. Second is a partially specular (PS) edge, such that the electron distribution is

$$\begin{aligned} g(\theta) &= g(-\theta) + \mathcal{D} \sin \theta \\ &\times \left[g(-\theta) - \frac{2}{\pi} \sin \theta \int_0^\pi \sin^2 \theta' g(-\theta') d\theta' \right], \end{aligned} \quad (7)$$

for all reflected angles $0 < \theta < \pi$, with $\mathcal{D} \lesssim 1$ a dispersion coefficient. In particular, if $\mathcal{D} \ll 1$, the edge is almost specular and a perfect slip boundary is obtained. For example, this model is able to reproduce the experimental results for uniform channels with DF boundaries and a uniform mean free path of $l_e = 20 \mu\text{m}$ for PdCoO_2 [36] (not shown for brevity). The definition of a mean free path is the common approach [36], which is followed even after the detailed first-principles calculations [29]. Therefore, current experimental evidence supports the assumption of an isotropic mean free path, while also suggesting that the anisotropy of the Fermi surface is the leading source for anisotropic electrical properties.

III. POISEUILLE AND COLLECTIVE FLOW

In this section, we analyze the Poiseuille flow in a very long uniform channel of width d . Figure 2 shows the flow profiles for the easy [Fig. 2(a)] and hard [Fig. 2(b)] transport directions, within a physical scenario between the ballistic and hydrodynamic regimes of transport, $d/l_e = 0.3$ and $d/l_{ee} = 1$. Experiments visualizing Poiseuille flow [6] are typically performed at finite temperatures, using the hydrodynamic description $l_{ee}^{\text{even}} = l_{ee}^{\text{odd}} = l_{ee}$, although the results would be equivalent under the tomographic approach [44]. DF boundaries are typically considered when studying Poiseuille-like profiles. Notice that our results fit the experimental observations in PdCoO_2 , where the largest (lowest) current is obtained for the easy (hard) direction. Moreover, our simulations also demonstrate that the profile curvature is also affected by the transport direction, being larger for the hard one ($\kappa = 0.34$)

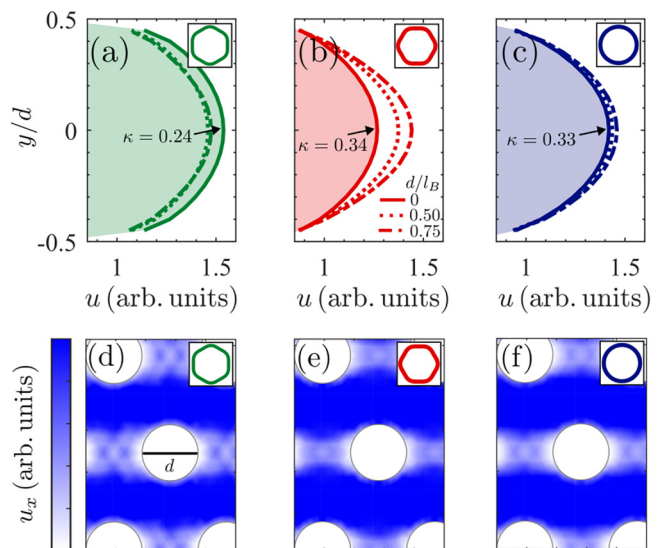


FIG. 2. Enhanced Poiseuille flow in the hard transport direction. The transverse velocity profile (a) in the easy transport direction, (b) in the hard transport direction, and (c) in an isotropic material for a uniform channel with DF boundaries and $d/l_e = 0.3$, $d/l_{ee} = 1$. We also show such profiles under the effect of a magnetic field, $d/l_B = 0.5$ (dotted lines) and $d/l_B = 0.75$ (dashed lines). (d)–(f) Color map of the propagation velocity in a honeycomb antidot superlattice simulated with the Boltzmann transport equation and DF edges for $d/l_e = 0.3$ and $d/l_{ee} = 0.5$.

than for the easy one ($\kappa = 0.24$). This is also in perfect agreement with previous results [29]. For completeness, we also study transport in an isotropic material in Fig. 2(c), whose profile curvature results are very similar to the one obtained in the hard direction.

Let us now explain why the transport direction determines the curvature. Consider the distribution of the electrons moving near the edge. The incident electrons contribute to the drift velocity, but those scattered from the edge flow equally in all directions, which reduces its contribution to the drift velocity. It is not until they move away from the edge that due to electron-electron collision or the accelerating potential, they recover their drift velocity and contribute to the electrical conduction. This explains the curved profiles in isotropic materials. However, the electrons in PdCoO_2 are only allowed to flow in six directions. When a device is aligned with an easy direction, there is a huge accumulation of electrons moving parallel to the channel, outshining the remaining directions. They rarely suffer edge scattering, so they keep the same drift velocity regardless of being near the edge or far away from it. Therefore, the overall current profile flattens. Conversely, when the device is set in the hard direction of transport, part of the electrons scatter from the boundaries, similarly to what happens in isotropic materials. This reduces the drift velocity near the edges and leads to a curved profile of electron velocities. An additional technical explanation based on the g distribution can also be provided. In the easy direction of transport, there is an accumulation of electrons parallel to the channel, so g is not a smooth function. In the hard direction, however, electrons, scattered from the boundaries, may flow in all directions and, as a result, g is a smoother function.

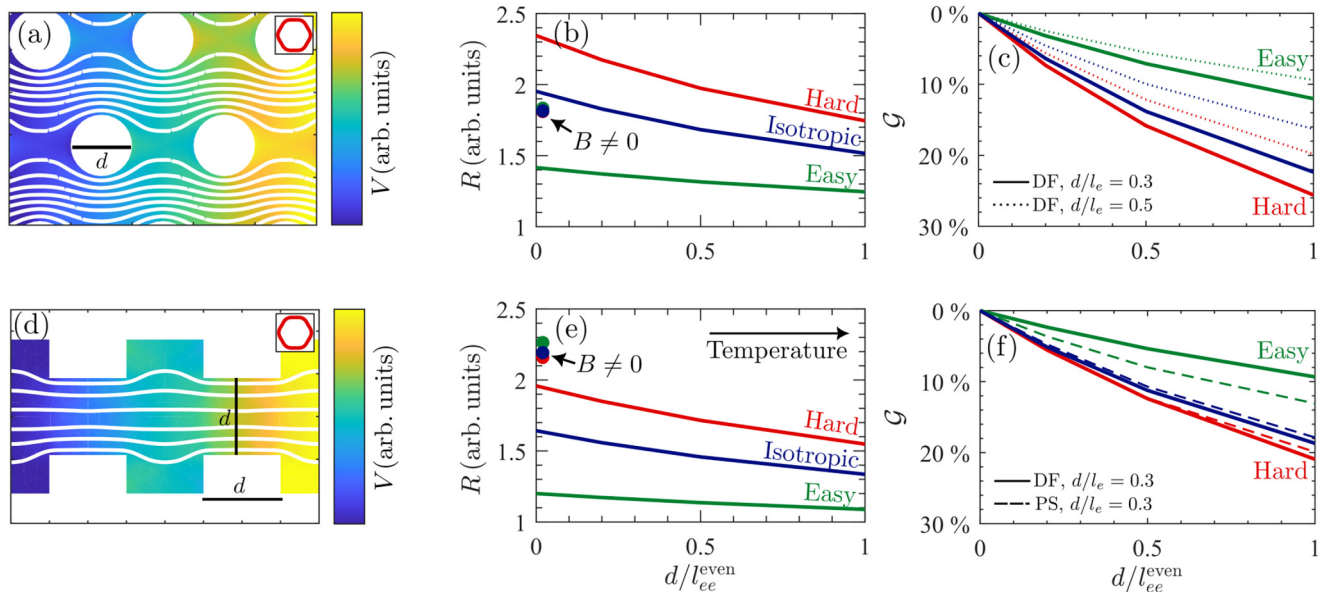


FIG. 3. Enhanced superballistic conduction in the hard direction. (a) Simulation of the Boltzmann transport equation, where colors account for the electric potential and streamlines are average electron trajectories in the honeycomb antidot superlattice with DF edges and $d/l_e = 0.3$, $d/l_{ee}^{\text{even}} = 0.5$, $d/l_{ee}^{\text{odd}} = 0$. (b) Resistance R of an antidot superlattice with DF edges and $d/l_e = 0.3$, when different transport directions are considered hard (red), easy (green), and isotropic (blue) transport. R decreases with increasing the magnitude d/l_{ee} , which favors electron-electron collisions. Solid circles show R when a magnetic field is applied, $d/l_B = 1$. (c) Gurzhi ratio $\mathcal{G} = 1 - R/R_{\text{max}}$ for the cases shown in (b) (solid lines) and with $d/l_e = 0.5$ (dotted lines). (d)–(f) The same magnitudes as in (a)–(c), but for a crenellated channel. For comparison, (f) presents results for PS boundaries with $\mathcal{D} \ll 1$ (dashed lines).

In the latter scenario, collective electron transport arises so the Boltzmann equation reduces to a hydrodynamic Navier-Stokes equation [39], and the curved profiles emerge naturally.

Notice that the differences between the easy and hard transport directions become more notorious the more we approach the ballistic regime, while they will blur if we go deeply into the hydrodynamic regime. Indeed, the modified Navier-Stokes equation that could be derived from Eq. (5) [39] would be the same for all transport directions. However, unless we are too deep into the hydrodynamic regime, the anisotropy affects the Boltzmann equation and largely determines the physical properties of the device. Another point to be considered is the role of the magnetic field [32], which can also induce hydrodynamic behavior [39,48,49]. We notice that unlike in the easy direction, in the hard direction low magnetic fields further increase the curvature of the Poiseuille profile. This opposite behavior can be considered as a different indicator to classify viscous electron flow in anisotropic materials.

Finally, we show that these conclusions are valid in other geometries. Let us focus on an antidot superlattice. The antidots have been sorted in a honeycomb fashion, or compact staking, with hexagonal symmetry. This defines a series of channels in the shape of hexagons and preferred transport directions every 60° . The latter could be easy or hard, depending on the axis of the anisotropic material. Although there is no formal definition of the Poiseuille flow beyond the uniform channel, we propose to look at the velocity field to study the degree of transport collectivity. As shown in Fig. 2(d), the flow in the easy direction occurs in parallel straight channels, such that the electrons do not follow the antidot geometry. However, in the hard direction presented in

Fig. 2(e), the electron trajectories are more curved and the velocity significantly increases in the regions between holes that are adjacent to the main flow. This is yet a clear indicator of collective flow in the hard transport direction, which is consistent with the results in the uniform channel. Lastly, Fig. 2(f) shows the electron flow in an isotropic antidot superlattice such that the electron trajectories result from a combination between those in the easy and hard directions with an intermediate degree of collectivity.

Altogether, we demonstrate that devices working in the hard transport direction facilitate the observation of hydrodynamics effects and, particularly, enhance the occurrence of the Poiseuille flow.

IV. SUPERBALLISTIC CONDUCTION

Superballistic conduction is another signature of viscous electron flow that has the most straightforward applications in circuits since it reduces dissipation [7–13]. Let us investigate how superballistic conduction is affected by the anisotropy. On the one hand, we need to consider a device with a non-trivial geometry, different from a uniform channel, to bend the electron flow and boost its collective response. On the other hand, the geometry has to establish well-defined easy and hard transport directions. The honeycomb antidot superlattice meets both criteria, as shown in the previous section. Figure 3(a) shows the bending of the carrier trajectories along the hard directions defined by the honeycomb.

As expected for the superballistic conduction, the increase in temperature, which favors electron-electron collisions, reduces the device resistance [see Fig. 3(b)]. It is at higher

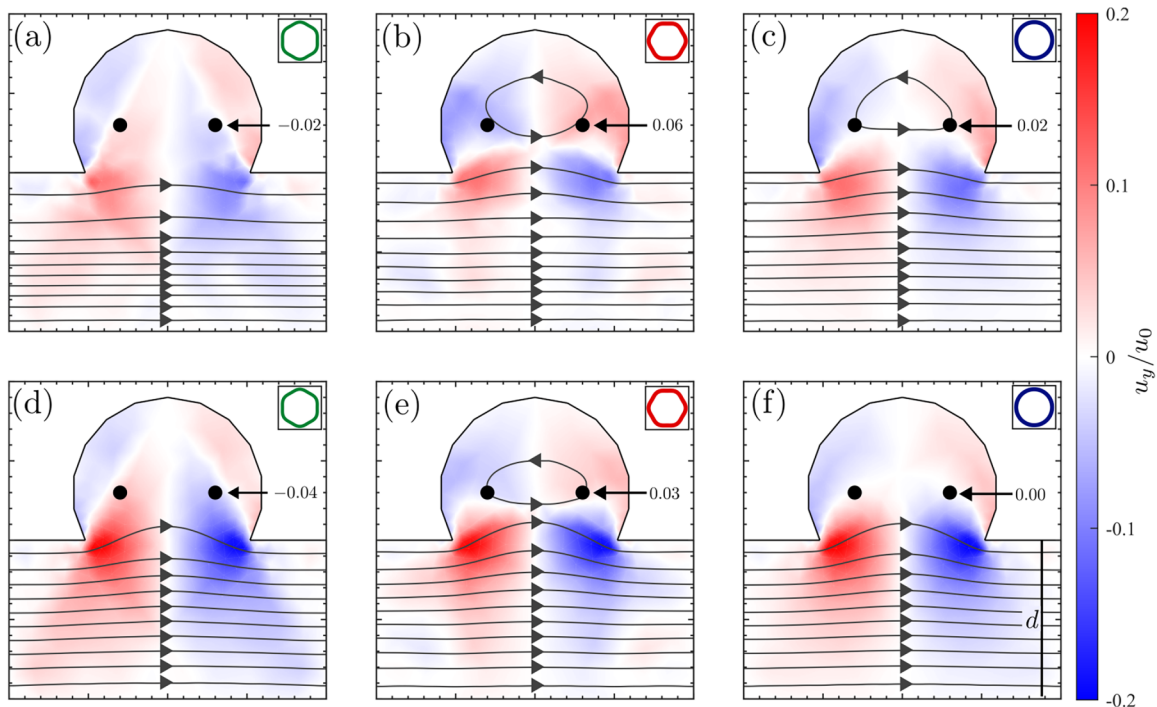


FIG. 4. Whirlpool formation enhances in the hard transport direction. Whirlpool formation in (a) the easy direction, (b) the hard direction, and (c) an isotropic material, after simulations of the Boltzmann equation near the ballistic regime, for $d/l_e = 0.1$, $d/l_{ee} = 0$, and DF edges. The flow in the channel is set from left to right. Specifically, the positive (negative) sign of the u_y velocity at half of the radius of the chamber (solid black circles) is used as an indicator of the formation (absence) of a whirlpool. We normalize the velocities to u_0 , the average drift velocity in the channel. Whirlpool in (d) the easy direction, (e) the hard direction, and (f) an isotropic material closer to the hydrodynamic regime of transport $d/l_e = 0.1$ and $d/l_{ee} = 1$.

temperatures where the decrease in l_e leads to an increase in the resistance [7]. The superballistic decrease in the resistance is much faster for the hard transport direction [see Fig. 3(c)]. The latter, which forbids ballistic trajectories along the honeycomb, favors the collective motion of electrons. Therefore, the transition from ballistic to hydrodynamic transport, which supports superballistic conduction, occurs more efficiently in the hard direction, yielding the steepest descent in the resistance. Due to the superballistic effect, the resistance in the hard direction (typically higher than in the easy one) eventually converges to the resistance in other directions as we go deeper into the hydrodynamic regime by decreasing l_{ee} . An additional magnetic field, which continuously rotates the electron trajectories in the antidot superlattice, removes the particular characteristics of transport in the easy and hard directions, leading to a common magnitude of the resistance [see symbols in Fig. 3(b)]. To quantify the superballistic effect, we also evaluate the Gurzhi ratio defined as $\mathcal{G} = 1 - R/R_{\max}$ [see Fig. 3(c)] to demonstrate that the superballistic conduction is enhanced in the hard direction. Besides, the same behavior is observed for another scattering rate d/l_e against impurities and phonons. For superballistic conduction, we mainly focus on the resistance decrease that occurs at very low temperatures compared to the Fermi temperature $T \ll T_F$. So, we take into account the tomographic description $l_{ee}^{\text{even}} \ll l_{ee}^{\text{odd}}$ of electron dynamics [12,44–46,50]. Lastly, we study superballistic conduction in a crenellated channel [see Fig. 3(d)]. As previously discussed for the antidot su-

perlattice, the resistance decay is also stronger in the hard transport direction [see Figs. 3(e) and 3(f)] and the resistances converge to the same value for all transport directions when a magnetic field is applied. In Fig. 3(f), we also demonstrate that it is the device geometry and the material anisotropy, and not the particular edge scattering, that mainly fixes the electron bent trajectories. Therefore, the effect is robust for different boundary conditions.

In short, superballistic conduction is strongly affected by anisotropy. A device in the hard direction exhibits a more conspicuous superballistic effect. The latter is particularly relevant when a device needs to operate in a hard transport direction. By hydrodynamics engineering, a hard transport direction can be transformed into an easier one, such that some of the detrimental transport effects of anisotropic materials can be overcome.

V. WHIRLPOOL FORMATION

Lastly, we consider the emergence of whirlpools in symmetry-broken devices since it has been considered a clear indication of collective transport [17]. Figure 4 shows the current whirlpools for several physical situations where the alignment of the device geometry and the material anisotropy is monitored. Let us focus on a regime of transport close to the ballistic one [51] ($d/l_e = 0.1$ and $d/l_{ee} \rightarrow 0$) in Figs. 4(a)–4(c), where the anisotropy of the material becomes more remarkable. Our simulations show that there is no

well-defined whirlpool formation in the easy transport direction [Fig. 4(a)], while it clearly appears and fills almost the whole chamber in the hard transport direction [Fig. 4(b)]. Even if we consider a case much closer to the hydrodynamic regime ($d/l_e = 0.1$ and $d/l_{ee} = 1.0$) in Figs. 4(d)–4(f), where the flow collectivity is increased due to favored electron-electron collisions, the different behavior regarding whirlpool formation is still appreciable in Figs. 4(d) and 4(e). Whirlpools are often studied at finite temperatures, so we use the hydrodynamic approach to electron dynamics ($J_{ee}^{\text{even}} = J_{ee}^{\text{odd}} = l_{ee}$), although an analog behavior is observed if we consider tomographic dynamics. Indeed, the map of velocities is completely different depending on the direction of transport, whether easy or hard. As previously proposed in Ref. [17], the sign of the velocity u_y at half of the radius of the chamber (see solid black circles in Fig. 4) is an indicator of the formation of a whirlpool. Particularly, if the flow in the channel is set from left to right, a negative (positive) sign in u_y is associated with the formation (absence) of a whirlpool.

This finding cannot only be used to reveal the direction of transport in anisotropic materials, easy or hard, but it mainly illustrates that experiments performed in the hard transport direction enhance the signatures of viscous flow.

VI. CONCLUSIONS

We analyzed the standard signatures of viscous electron flow when an anisotropic material is particularly placed in its easy and hard transport directions. Let us stress that at a first approach, since electron hydrodynamics can be described by the Navier-Stokes equation with isotropic viscosity tensors in hexagonal materials [37,52], its electrical properties were not expected to deviate from those of an isotropic crystal. Nevertheless, our simulations of the Boltzmann transport equation show that this is not the case for an intermediate regime of transport between the ballistic and the hydrodynamic ones, where a relevant degree of electron collective flow is present. This allows us to engineer a directional transport experiment to enhance the collective nature of electron flow in anisotropic materials. We show that anisotropic viscous electron flow can be studied in geometries beyond the standard uniform channel [36]. In geometrically engineered devices such as the honeycomb antidot superlattice, our study shows that well-established features for viscous flow, other than Poiseuille flow, also take place in nontrivial geometries. Therefore, the simulations of the Boltzmann equation prove that the concept of easy and hard transport directions arises beyond the uniform channel. Lastly, we demonstrate that viscous electron flow is enhanced in devices working in the hard transport direction, contrary to a general first intuition. Indeed, despite the lower dissipation in the easy transport direction, it is in the hard one where the collectivity of the electron flow is maximum.

In conclusion, the anisotropy itself can be considered as a different strategy to induce viscous electron flow [39]. We explored its effect on the performance of the Poiseuille flow, superballistic conduction, and electronic whirlpools, and we

found that such collective flow signatures enhance when the material and geometric anisotropy are smartly coordinated, this is, in the hard flow direction. Equivalently, if a device has to operate in the hard flow direction, viscous electron flow can play a major role in largely reducing its dissipation. It is worth mentioning that our results may be generalized to other anisotropic systems, such as bilayer graphene, for valleytronic applications [21]. Also, together with experimental progress in this material and visualizing techniques in PdCoO₂ [30,35,36], we expect our findings to be accompanied by experimental realizations of hydrodynamic transport in anisotropic materials.

VII. METHODS

The Boltzmann equation was solved numerically with a Galerkin conformal finite-element method [53]. We write

$$g(\mathbf{r}, \theta) = \sum_{n=1}^N \sum_{m=1}^M \phi_n(\mathbf{r}) \varphi_m(\theta), \quad (8)$$

where $\{\phi_n\}_{n=1}^N$ is the set of spatial tent functions and its products, defined on a triangular mesh [54] for each geometry. For the angular part, $\{\varphi_m\}_{m=1}^M$ is a set of periodic functions defined on $[0, 2\pi)$. $M = 32$ tent functions for the angular part were used. A uniform density of carriers is set in Eq. (5) to solve the resulting linear system with a least-squares approximation in MATLAB [55]. At the edges, the condition for PS boundaries (7) or $g(\theta) = 0$ for DF boundaries is imposed for reflected electrons. Periodic boundary conditions at the edges of the system were considered. We set the potential difference between two cells across the longitudinal direction and determine the Hall difference across the transverse direction with an additional equation that imposes no net flow across the transverse direction. Once the $g(\mathbf{r}, \theta)$ function is known, we compute the velocity field \mathbf{v} everywhere in space, such that its integral across the device is the current. The ratio between the voltage drop and the current gives the electrical resistance R . Lastly, we used numerical integration to find the total current and a fourth-order Runge-Kutta method to solve the electronic trajectories in the streamlines.

ACKNOWLEDGMENTS

We wish to acknowledge R. Brito, A. Cortijo, J. Bernabeu, and C. Ding for discussions. This work was supported by the “(MAD2D-CM)-UCM” project funded by Comunidad de Madrid, by the Recovery, Transformation and Resilience Plan, and by NextGenerationEU from the European Union and Agencia Estatal de Investigación of Spain (Grant No. PID2022-136285NB-C31). J.E. acknowledges support from the Spanish Ministerio de Ciencia, Innovación y Universidades (Grant No. FPU22/01039).

DATA AVAILABILITY

The data supporting these findings are available from the contact author upon reasonable request.

- [1] G. Varnavides, A. Yacoby, C. Felser, and P. Narang, Charge transport and hydrodynamics in materials, *Nat. Rev. Mater.* **8**, 726 (2023).
- [2] M. Polini and A. K. Geim, Viscous electron fluids, *Phys. Today* **73**(6), 28 (2020).
- [3] B. N. Narozhny, Hydrodynamic approach to two-dimensional electron systems, *Riv. Nuovo Cim.* **45**, 661 (2022).
- [4] L. Fritz and T. Scaffidi, Hydrodynamic electronic transport, *Annu. Rev. Condens. Matter Phys.* **15**, 17 (2024).
- [5] G. Baker, M. Moravec, and A. P. Mackenzie, A perspective on non-local electronic transport in metals: Viscous, ballistic, and beyond, *Ann. Phys.* **536**, 2400087 (2024).
- [6] J. A. Sulpizio, L. Ella, A. Rozen, J. Birkbeck, D. J. Perello, D. Dutta, M. Ben-Shalom, T. Taniguchi, K. Watanabe, T. Holder *et al.*, Visualizing Poiseuille flow of hydrodynamic electrons, *Nature (London)* **576**, 75 (2019).
- [7] R. K. Kumar, D. Bandurin, F. Pellegrino, Y. Cao, A. Principi, H. Guo, G. Auton, M. Ben Shalom, L. A. Ponomarenko, G. Falkovich *et al.*, Superballistic flow of viscous electron fluid through graphene constrictions, *Nat. Phys.* **13**, 1182 (2017).
- [8] A. C. Keser, D. Q. Wang, O. Klochan, D. Y. H. Ho, O. A. Tkachenko, V. A. Tkachenko, D. Culcer, S. Adam, I. Farrer, D. A. Ritchie *et al.*, Geometric control of universal hydrodynamic flow in a two-dimensional electron fluid, *Phys. Rev. X* **11**, 031030 (2021).
- [9] L. V. Ginzburg, C. Gold, M. P. Rössli, C. Reichl, M. Berl, W. Wegscheider, T. Ihn, and K. Ensslin, Superballistic electron flow through a point contact in a Ga[Al]As heterostructure, *Phys. Rev. Res.* **3**, 023033 (2021).
- [10] R. N. Gurzhi, Minimum of resistance in impurity-free conductors, *Zh. Eksp. Teor. Fiz.* **44**, 771 (1963) [*J. Expt. Theor. Phys.* **17**, 521 (1963)].
- [11] R. N. Gurzhi, Hydrodynamic effects in solids at low temperature, *Sov. Phys. Usp.* **11**, 255 (1968).
- [12] J. Estrada-Álvarez, J. Salvador-Sánchez, A. Pérez-Rodríguez, C. Sánchez-Sánchez, V. Clericò, D. Vaquero, K. Watanabe, T. Taniguchi, E. Diez, F. Domínguez-Adame *et al.*, Superballistic conduction in hydrodynamic antidot graphene superlattices, [arXiv:2407.04527](https://arxiv.org/abs/2407.04527) [*Phys. Rev. X* (to be published)].
- [13] A. Stern, T. Scaffidi, O. Reuven, C. Kumar, J. Birkbeck, and S. Ilani, How electron hydrodynamics can eliminate the Landauer-Sharvin resistance, *Phys. Rev. Lett.* **129**, 157701 (2022).
- [14] A. Aharon-Steinberg, T. Völkl, A. Kaplan, A. K. Pariari, I. Roy, T. Holder, Y. Wolf, A. Y. Meltzer, Y. Myasoedov, M. E. Huber *et al.*, Direct observation of vortices in an electron fluid, *Nature (London)* **607**, 74 (2022).
- [15] D. Bandurin, I. Torre, R. K. Kumar, M. Ben Shalom, A. Tomadin, A. Principi, G. Auton, E. Khestanova, K. Novoselov, I. Grigorieva *et al.*, Negative local resistance caused by viscous electron backflow in graphene, *Science* **351**, 1055 (2016).
- [16] D. A. Bandurin, A. V. Shytov, L. S. Levitov, R. K. Kumar, A. I. Berdyugin, M. Ben Shalom, I. V. Grigorieva, A. K. Geim, and G. Falkovich, Fluidity onset in graphene, *Nat. Commun.* **9**, 4533 (2018).
- [17] C. Ding, M. Palm, W. Huxter, T. Taniguchi, K. Watanabe, and C. Degen, Observation of current whirlpools in graphene at room temperature, *Science* **384**, 1134 (2024).
- [18] J. H. Farrell, N. Grisouard, and T. Scaffidi, Terahertz radiation from the Dyakonov-shur instability of hydrodynamic electrons in Corbino geometry, *Phys. Rev. B* **106**, 195432 (2022).
- [19] J. Estrada-Álvarez, E. Díaz, and F. Domínguez-Adame, Negative differential resistance of viscous electron flow in graphene, *2D Mater.* **12**, 015012 (2025).
- [20] W. Huang, T. Paul, M. Perrin, and M. Calame, Eliminating the channel resistance in two-dimensional systems using viscous charge flow, *2D Mater.* **11**, 033001 (2024).
- [21] J. Ingla-Aynés, A. L. Manesco, T. S. Ghiasi, K. Watanabe, T. Taniguchi, and H. S. van der Zant, A ballistic electron source with magnetically controlled valley polarization in bilayer graphene, *Phys. Rev. Lett.* **133**, 156301 (2024).
- [22] C. Gold, A. Knothe, A. Kurzmann, A. Garcia-Ruiz, K. Watanabe, T. Taniguchi, V. Fal'ko, K. Ensslin, and T. Ihn, Coherent jetting from a gate-defined channel in bilayer graphene, *Phys. Rev. Lett.* **127**, 046801 (2021).
- [23] J. R. Schaibley, H. Yu, G. Clark, P. Rivera, J. S. Ross, K. L. Seyler, W. Yao, and X. Xu, Valleytronics in 2D materials, *Nat. Rev. Mater.* **1**, 16055 (2016).
- [24] Y. Wang, G. Varnavides, R. Sundararaman, P. Anikeeva, J. Gooth, C. Felser, and P. Narang, Generalized design principles for hydrodynamic electron transport in anisotropic metals, *Phys. Rev. Mater.* **6**, 083802 (2022).
- [25] B. He, Y. Wang, M. Q. Arguilla, N. D. Cultrara, M. R. Scudder, J. E. Goldberger, W. Windl, and J. P. Heremans, The Fermi surface geometrical origin of axis-dependent conduction polarity in layered materials, *Nat. Mater.* **18**, 568 (2019).
- [26] G. Baker, T. W. Branch, J. S. Bobowski, J. Day, D. Valentinis, M. Oudah, P. McGuinness, S. Khim, P. Surówka, Y. Maeno *et al.*, Nonlocal electrodynamic in ultrapure PdCoO₂, *Phys. Rev. X* **14**, 011018 (2024).
- [27] X. Yao, Y. Xun, Z. Zhu, S. Zhao, and W. Li, Origin of the high electrical conductivity of the delafossite metal PdCoO₂, *Phys. Rev. B* **109**, 075110 (2024).
- [28] P. J. W. Moll, P. Kushwaha, N. Nandi, B. Schmidt, and A. P. Mackenzie, Evidence for hydrodynamic electron flow in PdCoO₂, *Science* **351**, 1061 (2016).
- [29] G. Varnavides, Y. Wang, P. J. W. Moll, P. Anikeeva, and P. Narang, Mesoscopic finite-size effects of unconventional electron transport in PdCoO₂, *Phys. Rev. Mater.* **6**, 045002 (2022).
- [30] P. H. McGuinness, E. Zhakina, M. König, M. D. Bachmann, C. Putzke, P. J. Moll, S. Khim, and A. P. Mackenzie, Low-symmetry nonlocal transport in microstructured squares of delafossite metals, *Proc. Natl. Acad. Sci. USA* **118**, e2113185118 (2021).
- [31] D. Valentinis, G. Baker, D. A. Bonn, and J. Schmalian, Kinetic theory of the non-local electrodynamic response in anisotropic metals: Skin effect in 2D systems, *Phys. Rev. Res.* **5**, 013212 (2023).
- [32] K. Wang, C. Guo, P. J. Moll, and T. Holder, Transverse voltage in anisotropic hydrodynamic conductors, [arXiv:2409.16088](https://arxiv.org/abs/2409.16088).
- [33] C. W. Hicks, A. S. Gibbs, A. P. Mackenzie, H. Takatsu, Y. Maeno, and E. A. Yelland, Quantum oscillations and high carrier mobility in the delafossite PdCoO₂, *Phys. Rev. Lett.* **109**, 116401 (2012).
- [34] H. Takatsu, J. J. Ishikawa, S. Yonezawa, H. Yoshino, T. Shishidou, T. Oguchi, K. Murata, and Y. Maeno, Extremely large magnetoresistance in the nonmagnetic metal PdCoO₂, *Phys. Rev. Lett.* **111**, 056601 (2013).

- [35] M. D. Bachmann, A. L. Sharpe, A. W. Barnard, C. Putzke, M. König, S. Khim, D. Goldhaber-Gordon, A. P. Mackenzie, and P. J. Moll, Super-geometric electron focusing on the hexagonal fermi surface of PdCoO₂, *Nat. Commun.* **10**, 5081 (2019).
- [36] M. D. Bachmann, A. L. Sharpe, G. Baker, A. W. Barnard, C. Putzke, T. Scaffidi, N. Nandi, P. H. McGuinness, E. Zhakina, M. Moravec *et al.*, Directional ballistic transport in the two-dimensional metal PdCoO₂, *Nat. Phys.* **18**, 819 (2022).
- [37] G. Varnavides, A. S. Jermyn, P. Anikeeva, C. Felser, and P. Narang, Electron hydrodynamics in anisotropic materials, *Nat. Commun.* **11**, 4710 (2020).
- [38] M. Qi and A. Lucas, Distinguishing viscous, ballistic, and diffusive current flows in anisotropic metals, *Phys. Rev. B* **104**, 195106 (2021).
- [39] J. Estrada-Álvarez, F. Domínguez-Adame, and E. Díaz, Alternative routes to electron hydrodynamics, *Commun. Phys.* **7**, 138 (2024).
- [40] T. Holder, R. Queiroz, T. Scaffidi, N. Silberstein, A. Rozen, J. A. Sulpizio, L. Ella, S. Ilani, and A. Stern, Ballistic and hydrodynamic magnetotransport in narrow channels, *Phys. Rev. B* **100**, 245305 (2019).
- [41] M. Di Ventra, *Electrical Transport in Nanoscale Systems* (Cambridge University Press, Cambridge, 2008).
- [42] M. J. M. de Jong and L. W. Molenkamp, Hydrodynamic electron flow in high-mobility wires, *Phys. Rev. B* **51**, 13389 (1995).
- [43] J. Callaway, Model for lattice thermal conductivity at low temperatures, *Phys. Rev.* **113**, 1046 (1959).
- [44] P. Ledwith, H. Guo, A. Shytov, and L. Levitov, Tomographic dynamics and scale-dependent viscosity in 2D electron systems, *Phys. Rev. Lett.* **123**, 116601 (2019).
- [45] S. Kryhin, Q. Hong, and L. Levitov, Linear-in-temperature conductance in two-dimensional electron fluids, [arXiv:2310.08556](https://arxiv.org/abs/2310.08556).
- [46] R. N. Gurzhi, A. N. Kalinenko, and A. I. Kopeliovich, Electron-electron collisions and a new hydrodynamic effect in two-dimensional electron gas, *Phys. Rev. Lett.* **74**, 3872 (1995).
- [47] E. I. Kiselev and J. Schmalian, Boundary conditions of viscous electron flow, *Phys. Rev. B* **99**, 035430 (2019).
- [48] A. I. Berdyugin, S. Xu, F. Pellegrino, R. K. Kumar, A. Principi, I. Torre, M. Ben Shalom, T. Taniguchi, K. Watanabe, I. Grigorieva *et al.*, Measuring Hall viscosity of graphene's electron fluid, *Science* **364**, 162 (2019).
- [49] A. N. Afanasiev, P. S. Alekseev, A. A. Greshnov, and M. A. Semina, Ballistic-hydrodynamic phase transition in flow of two-dimensional electrons, *Phys. Rev. B* **104**, 195415 (2021).
- [50] S. Kryhin, Q. Hong, and L. Levitov, Linear-in-temperature conductance in two-dimensional electron fluids, [arXiv:2310.08556](https://arxiv.org/abs/2310.08556).
- [51] K. G. Nazaryan and L. Levitov, Nonlocal conductivity, continued fractions, and current vortices in electron fluids, *Phys. Rev. B* **110**, 045147 (2024).
- [52] B. A. Braem, F. M. D. Pellegrino, A. Principi, M. Rössli, C. Gold, S. Hannel, J. V. Koski, M. Berl, W. Dietsche, W. Wegscheider *et al.*, Scanning gate microscopy in a viscous electron fluid, *Phys. Rev. B* **98**, 241304(R) (2018).
- [53] J. Whiteley, *Finite Element Methods, Mathematical Engineering* (Springer, New York, 2017).
- [54] D. Engwirda and D. Ivers, Off-centre Steiner points for Delaunay-refinement on curved surfaces, *Comput. Aid. Design* **72**, 157 (2016).
- [55] R. Barrett, M. Berry, T. F. Chan, J. Demmel, J. Donato, J. Dongarra, V. Eijkhout, R. Pozo, C. Romine, and H. Van der Vorst, *Templates for the Solution of Linear Systems: Building Blocks for Iterative Methods* (SIAM, 1994).